Vol. 85 No. 2 pp. 452–464 ACTA GEOLOGICA SINICA (English Edition) April 2011

Terrestrial Mio-Pliocene Boundary in the Linxia Basin, Gansu, China

DENG Tao[1, *], HOU Sukuan[1, 2], SHI Qinqin[1, 2], CHEN Shaokun[1, 2], HE Wen[3] and CHEN Shanqin[3]

1 *Key Laboratory of Evolutionary Systematics of Vertebrates, Institute of Vertebrate Paleontology and Paleoanthropology, the Chinese Academy of Sciences, Beijing 100044, China*
2 *Graduate School of the Chinese Academy of Sciences, Beijing 100039, China*
3 *Hezheng Paleozoological Museum, Hezheng, Gansu 731200, China*

Abstract: The Lower Pliocene of the Linxia Basin in Gansu Province is one of only a few representative sections for the Early Pliocene sedimentary records in northern China, and even in East Asia. Recently, abundant mammalian fossils were found from the base of red clays of the Lower Pliocene Hewangjia Formation at Duikang in Guanghe County within this basin. Previously, the Pliocene mammals were sparsely found in China, and most were collected from fluvial and lacustrine deposits in the eastern Loess Plateau. Mammals from the widely distributed Pliocene *Hipparion* Red Clay are less in number. The known fossils from Duikang include 20 species and belong to the Shilidun Fauna. Their faunal components are similar to the Early Pliocene Gaozhuang Fauna from Yushe, Shanxi. On the other hand, some taxa from Duikang have not been found in the Gaozhuang Fauna, are slightly more primitive in evolutionary level, and appeared mainly in the Late Miocene. As a result, the age of the Duikang fossils may be slightly earlier than that of the Gaozhuang Fauna and closer to the lower boundary of the Pliocene. The Duikang fossiliferous bed is 0.8 m above the top of the Late Miocene Liushu Formation, and the first occurrence of the three-toed horse *Hipparion pater* can be regarded as a biostratigraphical marker of the Miocene/Pliocene boundary. In conclusion, Duikang is an ideal candidate locality to establish as the stratotype of the lower boundary of the Chinese terrestrial Pliocene.

Key words: Miocene, Pliocene, boundary stratotype, mammalian fauna, *Hipparion* Red Clay, Linxia Basin

1 Introduction

The Linxia Basin in Gansu Province is very rich in mammalian fossils from the Late Oligocene *Dzungariotherium* fauna to the Early Pleistocene *Equus* fauna. Among them, the Late Miocene *Hipparion* fauna has the most massive fossil specimens and localities. However, the Pliocene fossil localities were rarely found in the Linxia Basin previously, producing very few taxa and specimens. Recently, a 45 m long fossil lens was discovered from the red clays of the Early Pliocene Hewangjia Formation at Duikang in Zhuangheji Township, Guanghe County (Fig. 1). Cutting into many blocks that were 1 m long, the whole lens was successively excavated and moved into the Hezheng Paleozoological Museum. Some taxa in the large-sized lens were also found at Shilidun and Yinchuan in the Linxia Basin several years ago (Deng et al., 2004a, b; Deng, 2005), and some taxa are very similar to the large mammals of the Gaozhuang Fauna from Yushe, Shanxi (Deng et al., 2010). Duikang is not far from Shilidun, with a linear distance of only 4.75 km. The Duikang fossils belong to the Early Pliocene Shilidun Fauna. In China, the Early Pliocene fossil localities are infrequent, especially localities of large mammals, which, in the past, were found mainly from the fluvial and lacustrine deposits in eastern Loess Plateau, typically represented by the Yushe Basin in Shanxi Province (Qiu, 1987; Qiu et al., 1987; Flynn et al., 1991). The Pliocene fossils from red clays are very scarce. This has been a puzzle to Chinese researchers of the Neogene mammalian fossils, because the traditional methods of stratigraphical correlations depending on large mammals are difficult to use in the Pliocene strata of red clays. We investigated the fossil locality at Duikang, and initially identified the fossils collected from this fossiliferous lens. Our investigation proves that the red clays of the Late Miocene Liushu and Early Pliocene Hewangjia formations are well exposed at Duikang.

* Corresponding author. E-mail: dengtao@ivpp.ac.cn

Besides the huge fossiliferous lens in the Hewangjia Formation, mammalian fossils are produced from the greyish-green mudstones in the top part of the Liushu Formation. The fossils from the Hewangjia lens are very abundant and include some new taxa; their age may be slightly earlier than that of the Gaozhuang Fauna.

In the past, Yushe Zone II and the Jinglean Age were used to represent the Chinese Pliocene mammalian ages. However, the mammals of Yushe Zone II did not come from a certain locality or localities, or from an exact horizon. They were composited by Teilhard de Chardin depending on his judgment for their evolutionary levels, among which there were fossils from not only lower but also upper horizons (Teilhard de Chardin and Young, 1933; Licent and Trassaert, 1935). The Jinglean Age was established based on several mammalian species from the west of Hefeng in Jingle, Shanxi, including the true elephant whose age was impossibly earlier than 3 Ma, and some more primitive taxa (Teilhard de Chardin and Young, 1930). Other Pliocene large mammal assemblages were collected from Youhe in Weinan, Shaanxi, Dongyaozitou in Yuxian, Hebei, and Leijiahe and Renjiagou in Lingtai, Gansu. Among them, only the Gaozhuang Fauna belongs to the Early Pliocene, and only Hefeng and Renjiagou faunas are collected from red clay deposits. The other faunas were found from the Late Pliocene fluvial and lacustrine deposits.

In 1930, Teilhard de Chardin and Young discovered mammalian fossils during their investigation of red clays in the Jingle area. They described the red clay (or loam) deposits as three layers named A, B, and C. The Hefeng Fauna was collected from Red Clay A and included *Hipparion houfenense*, *Antilospira licenti*, *Gazella blacki*, *Cervus* sp., Rhinocerotidae gen. indet., *Elephas* sp., etc. (Teilhard de Chardin and Young, 1930). Chen (1994) found two other mammalian species, i.e. *Nyctereutes sinensis* and *Metailurus* cf. *major* from Hefeng. Yue and Zhang (1998) used magnetostratigraphic analysis, which indicated that the age of Red Clay A is 3.0–2.5 Ma, belonging to the Late Pliocene. Zhang et al. (1999) reported the mammalian fossils excavated from red clays at Renjiagou in Lingtai, Gansu, which included *Chardinomys* sp., *Nyctereutes sinensis*, Gomphotheriidae gen. indet., *Hipparion houfenense*, Rhinocerotidae gen. indet., *Paracamelus* sp., *Gazella* sp., *G. blacki*, and *Antilospira licenti*. The magnetostratigraphic age was 3.4–3.5 Ma, i.e. the early Late Pliocene.

The fossils from Duikang are much richer in taxa and earlier in age than those from red clays at Hefeng and Renjiagou. As a result, the Linxia Basin is a unique area to find mammalian fossils from the Early Pliocene red clays, which provides an ideal candidate stratotype in order to establish the lower boundary of the Chinese terrestrial Pliocene.

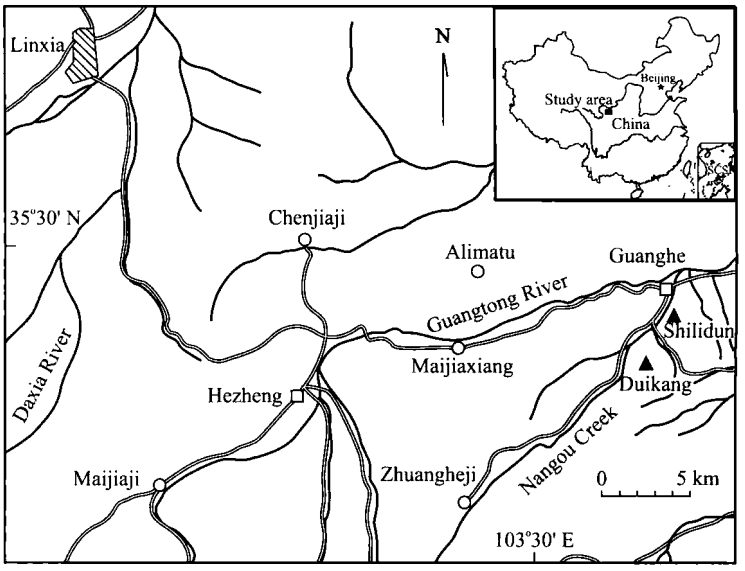

Fig. 1. Location map of the studied area in the Linxia Basin.

2 Geological Setting

The Linxia Basin is located on the triple-junction of the northeastern Tibetan Plateau, West Qinling and the Loess Plateau, delineated by high angle deep thrusts. It is a sub-basin of the Longzhong Basin. The lateral extent of the Linxia Basin is marked by structural boundaries on the northern, western, and southern edges, but is poorly determined towards the east. The basin is filled with 700–2000 m of thick late Cenozoic deposits, which are mainly red in color and dominated by lacustrine siltstones and mudstones punctured by fluvial conglomerates or sandstones, and 30–200 m of the Quaternary loess. The Yellow River and its main tributaries, the Daxia and Tao rivers, intermittently incise the whole late Cenozoic strata and expose complete sections, rendering them convenient for study (Li et al., 1995). To the west and south, the major basin-bounding faults within the Tibetan Plateau are the Leijishan and North Qinling faults, respectively. The Cenozoic deposits of the Linxia Basin begin with the Late Eocene deposits. The sedimentary rocks of the Linxia Basin overlap the Cretaceous sedimentary rocks in the Maxian Mountains to the north. Throughout the central part of the Linxia Basin, the oldest deposits were laid down on the granite of an inferred Paleozoic age. Southwest of the Linxia Basin, the Tibetan Plateau consists of Devonian-Permian terrestrial and marine deposits and Triassic submarine fan deposits (Zhang et al., 2010), which were shed by the east-southeast striking Qinling mountain belt to

the east of the plateau (Fang et al., 2003).

Prior to the 1960s, the Cenozoic deposits of the Linxia Basin were simply called the Gansu Series. In 1965, the First Regional Geologic Survey Team of the Gansu Geological Bureau created a new name, Linxia Fm., for the whole Cenozoic sequence, subdivided it into four members (1 to 4), and dated the whole sequence as Pliocene based on some *Hipparion* fossils found in the upper-most part of the sequence. Qiu et al. (1990) created a new formation, Jiaozigou Formation, for the lower part of the section, corresponding to the members 1 and 2 of the Linxia Formation, and thus, restricted the Linxia Formation to the members 3 and 4. A research group from Lanzhou University resubdivided the late Cenozoic deposits of the Linxia Basin in 1990s, nominating a series of new lithological units and dating them mainly by the paleomagnetic method (Li et al., 1995; Fang et al., 1997, 2003). Deng et al. (2004a, b) and Qiu et al. (2004b) revised the lithological sequence, and adopted the following units: the Oligocene Tala and Jiaozigou, the Miocene Shangzhuang, Dongxiang, Hujialiang, and Liushu, the Pliocene Hewangjia and Jishi, and the Early Pleistocene Wucheng formations.

Fig. 2. Photo of the Duikang section in the Linxia Basin, showing the position of the fossiliferous lens in the Hewangjia Formation.

Both the Late Miocene Liushu and Early Pliocene Hewangjia formations are red clay deposits, bearing abundant fossils of the *Hipparion* fauna. Sedimentological and geochemical studies proved that this Neogene red clay is windblown in origin as is the overlying Pleistocene loess (Ding et al., 1998; Guo et al., 2001). One of the most striking features of the red clay sequence is the existence of many horizontal carbonate nodule horizons. The thickness of these horizons ranges from 10 cm to >100 cm, with most of the nodules being <10 cm in diameter. The cement matrix within most of the nodule horizons is a reddish, weathered soil material.

The Liushu Formation consists of light yellowish-brown carbonate-cemented siltstones intercalated with a few thin beds of mudstones and marlites, developing substantial mottles and big carbonate nodules. The Hewangjia Formation consists of yellowish-brown calcareous mudstones encompassing big carbonate nodules intercalated by many marlite beds, with basal conglomerates that are thicker in the western part of the Linxia Basin and thinner in the eastern.

The strata at Shilidun in Guanghe County are well exposed and include the Hujialiang, Liushu, Hewangjia, and Jishi formations. The fossiliferous bed at Shilidun is situated within the red clays, 3 m above the basal conglomerate of the Hewangjia Formation, and contains *Hystrix gansuensis*, *Alilepus* sp., *Promephitis* sp., *Chasmaporthetes* sp., *Hyaenictitherium wongii*, *Cervavitus novorossiae*, *Palaeotragus* sp., *Samotherium* sp., *Protoryx* sp., *Sinotragus* sp., and *Capricornis* sp. (Deng, 2004a, 2009).

3 Duikang Section

Duikang is located 6.5 km southwest of the Guanghe County seat, near Nangou Creek, a branch of the Guangtong River (Fig. 1). The fossiliferous locality is situated on the southwest escarpment of the upper Shuimo Gully on the southeast slope of Nangou Creek, with an elevation of 2153 m (Fig. 2). The Shuimo Gully's outlet to Nangou Creek is located at the village Xinzhuang, with an elevation of 2060 m. Our measured section begins from the lower end of the Shuimo Gully (35°25'39.8"N, 103°32'48.3"E) and terminates on the upper end of this gully (35°25'22.1"N, 103°32'59.6"E), with a total thickness of >84 m. This section includes two informations: the lower part is the Late Miocene Liushu Formation whose top greyish-green mudstones contain *Hipparion* sp. and

Sinotragus sp., and the upper part is the Early Pliocene Hewangjia Formation, whose basal red clays contain a huge fossiliferous lens (Fig. 3). The section is capped by the Late Pleistocene Malan Loess. It is described from top to bottom as follows:

Late Pleistocene Malan Loess

13. Greyish-white silty clays, bearing a lot of plant roots and snail fossils

----------Disconformity----------

Early Pliocene Hewangjia Formation

12. Interbedded brownish-yellow silty mudstones and muddy siltstones with calcareous cement. A single mudstone bed is 1.5 m thick, with many greyish-green marlite bands, and a single siltstone bed is 60 cm thick. Not to top. >15 m

11. Brownish-red silty mudstones intercalating many brownish-yellow calcareous nodule beds. A single mudstone bed is about 40 cm thick, and a single nodule bed is 10–20 cm thick. The fossiliferous lens described in this paper was excavated from the bottom of this layer. 10.8 m

Late Miocene Liushu Formation

10. Blocky brownish-yellow calcareous siltstones with hard cementation, containing rich fine crystalline calcites. Iron-manganese components have a dotted distribution and form coatings on fissure surfaces. 1.66 m

9. Thick-bedded greyish-green sandstone and conglomerate lenses, changing into interbedded brownish-red silty mudstones and muddy siltstones. The lenses have partial brownish-yellow impregnation, with moderate psephicity and sorting, and hard cementation. The surfaces of gravels are frequently oxidized to red. The top of this layer consists of greyish-green mudstones with a thickness of 56 cm, bearing sandy components, and partly containing coarse sands or fine gravels. *Hipparion* sp. and *Sinotragus* sp. were discovered from the top part of this layer. 8.62 m

8. Thick-bedded light brownish-red silty mudstones banding yellowish-brown muddy siltstones, with small greyish-green sandstone and conglomerate lenses. 12.75 m

7. Thin-bedded greyish-green sandstones and conglomerates in lower part, with high psephicity, loose cementation, and poor sorting; two thick calcareous siltstone beds banding a muddy siltstone bed in the middle part, with hard cementation and richly dotted with crystalline calcites; greyish-green sandstones and conglomerates in the upper part, changing to large lenses with high psephicity and loose cementation. ~8 m

6. Thick-bedded brownish-red muddy siltstones banding two thick calcareous siltstone beds, with a small amount of fine gravels, hard cementation, crystalline vein, and miarolitic calcites. 6.8 m

5. Interbedded light yellowish-brown and brownish-red muddy siltstones, and interbedded brownish-red muddy siltstones and calcareous siltstones. Each bed is about 50 cm thick. Muddy siltstone beds contain white amorphous calcites and reticular iron-manganese coatings. Calcareous siltstones have hard cementation, containing many fine grains with diameters of 2–4 mm. 6.93 m.

4. Light greyish-green muddy siltstones with dotted iron-manganese components, containing calcareous nodules with diameters from 3 cm to >10 cm. 0.71 m.

3. Interbedded brownish-red muddy and calcareous siltstones with iron-manganese coatings. The calcareous siltstones have hard cementation, containing worm tubes and plant roots that are filled by muddy components. 8.95 m.

2. Greyish-green siltstones and fine sandstones with dotted iron-manganese components, containing quartzose coarse sands or fine gravels as well as white amorphous calcites. 1.24 m.

1. Light brownish-red silty mudstones dotted with iron-manganese components banding a 20 cm thick greyish-green siltstone bed with hard cementation. Not to bottom. >2.72 m

4 Mammalian Fossils

The following is a preliminary list of the mammalian fossils from Duikang, including Rodentia: *Hystrix gansuensis*; Lagomorpha: *Alilepus* sp.; Carnivora: *Sinictis dolichognathus*, *Parataxidea sinensis*, *Hyaenictitherium wongii*, *Adcrocuta eximia*, *Chasmaporthetes kani*, and *Felis* sp.; Perissodactyla: *Hipparion hippidiodus*, *H. platyodus*, *H. licenti*, *H.* (*Proboscidipparion*) *pater*, *Shansirhinus ringstroemi*, *Hesperotherium* sp., and *Ancylotherium* sp.; Artiodactyla: *Cervavitus novorossiae*, *Palaeotragus microdon*, *Samotherium* sp., *Sinotragus* sp., and *Gazella blacki*.

The above-mentioned 20 mammal species can be divided into two groups: (1) forms same as or close to those of the Gaozhuang Fauna, such as *Chasmaporthetes kani*, *Hipparion licenti*, *H. platyodus*, *H. pater*, *Shansirhinus ringstroemi*, *Cervavitus novorossiae*, *Hystrix gansuensis*, *Hyaenictitherium wongii*, and *Gazella blacki*; (2) forms not found in the Gaozhuang Fauna, such as *Sinictis dolichognathus*, *Parataxidea sinensis*, *Adcrocuta eximia*, *Felis* sp., *Hipparion hippidiodus*, *Ancylotherium* sp., *Palaeotragus microdon*, *Samotherium* sp., and *Sinotragus* sp., which were at a slightly lower evolutionary level and appeared mainly in the Late Miocene. Important characters of the fossil species from Duikang are briefly described as follows.

Hystrix gansuensis is a large-sized porcupine (Fig. 4a). The nasals are enlarged, and their anterior ends are more retracted than those of the premaxillae. The nasals and

premaxillae form an obvious nasal notch. The frontal surface is broad, with a prominent central part of the posterior margin. The skull roof is strongly constricted in the parietal area. The parietal bones are small and their posterior margins have a wide V-shaped depression that contains the triangular interparietal bone. The parietal crests are weak and rapidly convergent. In lateral view, the swollen frontal bones form a steep slope from the parietal bones. The diastema between I2 and P4 is long. The muzzle is high. The infraorbital foramen is large, with a posterior margin above the middle of M1. The orbit is large and its anterior rim is above the posterior margin of M2, lacking a postorbital process. The zygomatic process of the zygomatic bone is strongly posteriorly extended, and even exceeding the posterior end of the zygomatic arch. The zygomatic process of the temporal bone is short, not reaching the middle of the orbit. The horizontal ramus of the mandible is narrow and long. The diastema between i2 and p4 is shorter than the length of the cheek tooth row. The mental foramen is located under the anterior margin of p4. The masseteric fossa is shallow, with a weak upper masseteric ridge, but has a well-developed lower masseteric ridge, curvedly extending superio-anteriorly and reaching the anterior margin of p4. The cheek teeth are medium-hypsodont.

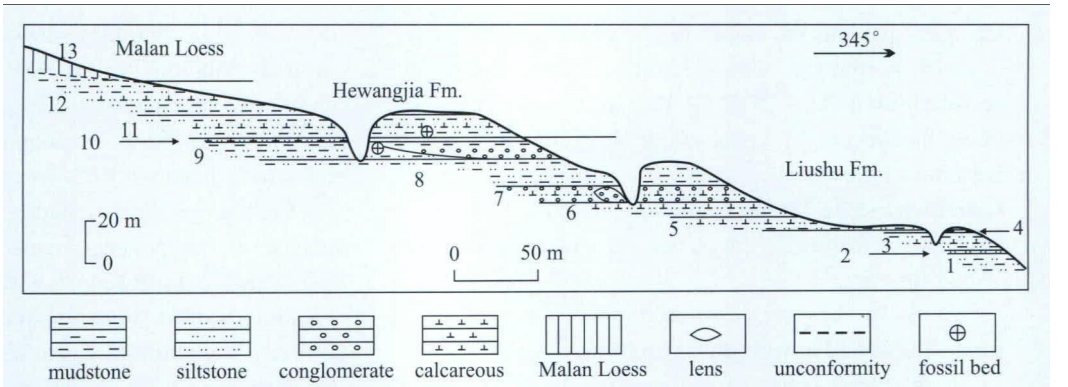

Fig. 3. Schematic section at Duikang in Guanghe County, Gansu Province.

Sinictis dolichognathus is a large-sized mustelid. The Duikang specimen is larger than the Baode specimens (Zdansky, 1924). In dorsal view, the postorbital region is obviously constricted, and the temporal lines are rapidly convergent, uniting into a high sagittal crest. In lateral view, the muzzle and nostrils are low. There is a marked depression in front of the orbit, which makes the orbital border clear. The anterior rim of the orbit is above the anterior root of P4. The infraorbital foramen is narrow and moderate in size, and is located under the front of the orbit and above the anterior part of P4. The zygomatic arches are fine. The lower margin of the horizontal ramus of the mandible is roundly curved at front and straight at back. There are two mental foramens under p2 and p3, respectively. I1 and I2 are very small, but I3 is markedly enlarged. C is very large and long, and its tip does not exceed the lower margin of the horizontal ramus in occlusion. There are diastemata between the premolars. P1 is small and close to C. P2 is double-rooted, and its main cusp has a straight anterior margin and a concave posterior margin. P3 is similar to P2 in shape, but much larger than P2 in size. P4 is long, and its parastyle is cingulum-like; the paracone is high, with an oblique anterior margin that is much longer than the posterior margin, with a rounded carnassial notch from the metastyle. In lateral view, both the paracone and metacone are low, but the former is obviously larger and higher than the latter, between which a groove exists; the labial cingulum is absent. Both p3 and p4 have a single cusp and double roots.

Parataxidea sinensis is a small badger with a short muzzle (Fig. 4b). The nasals are wide at the front and back, but constricted at the middle. In dorsal view, the sagittal groove is wide and shallow. The temporal lines are rapidly convergent, forming a weak sagittal crest. In lateral view, the dorsal border is posterio-superiorly oblique and slightly concave. The zygomatic arches are strongly curved. Both postorbital processes of the zygomatic and frontal bones are well-developed. The infraorbital foramen is located above the P3/P4 boundary and under the anterior rim of the orbit. The lower margin of the orbit is located at the middle of the height of the skull. The labial surface of the mandibular symphysis is convex and rough, with a marked sagittal groove. The horizontal ramus is narrow, and its lower margin is almost straight behind p3. The mental foramen is large, and is located under the anterior margin of p2 and near the lower margin of the horizontal ramus. The incisors are strong. I/i1 are similar to I/i2 in size, while I/i3 are markedly enlarged. C is straightly inferiorly extended, and c is exterio-superiorly extended. The labial cingulum is absent on the cheek teeth. P/p2 and P/p3 are robust, with a high main cusp for each of them. P4 is the longest among the upper cheek teeth; the paracone is conical and slightly higher than the metacone, with a long anterior margin and a concave base; the parastyle is very low and tiny; there is a groove between the metacone and paracone. M1 is transversely wide and low, and convex at the labial side.

Hyaenictitherium wongii: this hyaena from Duikang is larger than that from Baode in size. In dorsal view, the nasals are narrow and long, exceeding the anterior rim of the orbit. The sagittal depression of the frontal bones

Fig. 4. Mammalian fossils from the basal part of the Hewangjia Formation at Duikang in the Linxia Basin. Scale bars = 5 cm.
(a) Skull and mandible of *Hystrix gansuensis*, lateral view; (b) Skull and mandible of *Parataxidea sinensis*, lateral view; (c) Right upper jaw with dentition of *Chasmaporthetes kani*, occlusal view; (d) Right mandible of *Hyaenictitherium wongii*, lateral view; (e) Skull of *Ancylotherium* sp., lateral view; (f) Left upper jaw with cheek teeth of *Hipparion pater*, occlusal view; (g) Right upper cheek teeth of *Hipparion platyodus*, occlusal view; (h) Left lower cheek teeth of *Hipparion pater*, occlusal view.

between the parietal crests is marked. The braincase is narrow and the zygomatic arches are strongly expanded laterally. In lateral view, the orbit is round, with a sharp lower rim, and its anterior rim is located above the middle of P4. The infraorbital foramen is rounded and located above P3. There is a long distance between the postorbital processes of the frontal and zygomatic bones, so that the orbit has a large posterior opening. The mental foramen is large in size and oval in shape, and is located under the p1/p2 boundary. The anterio-inferior corner of the masseteric

fossa is rounded and far from m1 (Fig. 4d). C is thin and long, with an oval cross section and a marked labial cingulum. P2 has a high and relatively flat main cusp, and a well-developed metastyle. P3 is similar to P2 in shape, but is much larger than P2 in size. P4 is prolonged, with a length of 25.4 mm; on the labial side, there is a depression between the parastyle and paracone, and the main cusp is very flat. The parastyle is as long as 2/3 of the paracone, and the metastyle is approximately as long as the metacone. The c is slender and posteriorly curved; there is a wide and rounded ridge on the middle of the labial surface, before and behind which there is a fine groove, respectively. The diastema of c-p1 is long, with a length of 6.3 mm. The main cusps of the lower premolars are high, with a straight anterior margin and a concave posterior margin. The p1 is rudimental and tiny. The p4 has well-developed para- and meta-stylids; the parastylid is conical, and the metastylid is crestiform; the lingual cingulum is marked. The paraconid of m1 has the same length as the protoconid; the anterior part of the lingual cingulum is obvious; the meta- and entoconids are strong cones and the talonid is well-developed.

Adcrocuta eximia is a large-sized hyaena. The length from the anterior margin of I1 to the posterior margin of M1 is 129.8 mm, the length of I1-P4 is 134.2 mm, and the length of P1–P4 is 88.2 mm. The palatal surface is broad and slightly concave, and the palatal fissure is particularly wide and anteriorly convergent. The posterior palatine foramen is large and rounded, and is located at the level in front of P2. The upper dental formula is 3.1.4.1. The outline of I1 is narrow and oval. I2 is slightly larger than I1, and its posterior margin has a pair of marked supplementary cusps. I3 is very large and caniniform, twice as large as I1 in size, with a distinct posterior cingulum and a well-developed accessory cusp on its exterio-posterior side. In lateral view, the crown of C is straight and extends anterio-inferiorly. P1–P4 are arranged in a straight line and interspaced by short diastemata. P1 is small and conical, shifted near the lingual side of C; the lingual and labial surfaces are convex, the anterior and posterior ridges are well-developed, and the lingual cingulum is remarkable. P2 has a convex labial surface, a concave lingual surface, a rounded anterior margin, a small and low metastyle that is separated by a shallow groove from the main cusp, and a weak cingulum. P3 is notably more robust than P2 in size, but similar to P2 in shape; the anterior edge is distinct and lingually oblique, and the parastyle is weak. The wearing facets of P2 and P3 are horizontal. P4 is 36.8 mm long; the protocone is a small curved ridge; the parastyle is shorter than the paracone that is shorter than the metastyle; the parastyle is sturdy, with a horizontal wearing facet; the wearing facets of the paracone and metastyle are lingually oblique, and the latter is narrow and long. M1 is small and transversely long; the para- and meta-cones are indistinct, and the protocone is large.

Chasmaporthetes kani: this hyaena has anterio-posteriorly flat canines with slightly posteriorly-bended crowns (Fig. 4c). The cheek teeth are high-crowned. The premolars are more slicing, with well-developed accessory cusps that are distinctly apart from the main cusps. P1 is large, high and flat, with a flat lingual surface. P2 is the most obliquely positioned in the cheek tooth row, with a 30° angle between its midline and the row; the main cusps are labially convex and lingually flat; the parastyle is strong and obviously extending lingually. P3 is very similar to P2 in shape, but has a much larger size, a more oblique position, and a more posteriorly-shifted pre-endostyle. The labial ridge of P4 is deeply concave between the parastyle and paracone, with a distinct groove at the corresponding position of the labial wall; three main cusps on the labial ridge are relatively flat; the parastyle is as long as half of the paracone, and the metastyle is approximately as long as the paracone, with a concave labial wall; the protocone is high, lingually rounded and labially flat, with a deep depression apart from the labial ridge. M1 is very large, transversely wide, and located on the posterior-lingual side of P4; the protocone is well-developed and similar to that of P4 in shape. The c is slightly posteriorly curved. The main cusps of the lower premolars are high and robust, and there is a lack of labial cingulum. The p1 is tiny and single-rooted, and is tightly close to c. The p2 has diastemata separating it from p1 and p3. The p2 and p3 lack parastylids, and their metastylids are much lower than the main cusps. The p4 has a well-developed and highly positioned parastylid and a large metastyle. The Duikang specimen of *C. kani* has P1/p1, but the Yushe specimens have none (Qiu, 1987), which indicates that the former is more primitive.

Felis sp. from Duikang is a small-sized felid with a total cranial length of about 110 mm. The skull is short and high. The parietal lines are faint and slowly convergent, forming a short sagittal crest. The frontal surface is broad and convex. The postorbital constriction is unobvious and the braincase is enlarged. The zygomatic arches are strongly laterally expanded, with a maximum width between the postglenoid processes. In lateral view, the depression in front of the orbit is shallow, containing the muffle and upper lip levator in life. The infraorbital foramen is located under the front of the orbit, at the level of the middle of P3. The anterior rim of the orbit is located above the posterior root of P4. The postorbital process is moderately long. I3 is remarkably enlarged and caniniform. C is located on the exterio-superior side of the incisors, and is robust, conical, and slightly posteriorly curved. P2 is absent. The two premolars are simply structured. The main cusp of P3 is high and sharp, with a straight and oblique anterior margin

and a slightly concave base.

Hipparion (*Proboscidipparion*) *pater*: this three-toed horse lacks a preorbital fossa. The nasal notch is rounded, with a bottom above the middle of M2. The cheek teeth become narrow from P2 to M3 gradually, and have long and biforked plications. The protocone is small and narrowly rounded, with a flat lingual margin, and is smallest on P2 and longest on M3. The hypocone is short, the hypoconal groove is distinct, and the hypoconal constriction is weak. On an upper jaw, each hypocone is strongly constricted forming an oval shape, with a very deep hypoconal groove and constriction (Fig. 4f). This configuration is also seen on a specimen from Yushe (Qiu et al., 1987, fig. 13). On the premolars, the parastyle is wide, with two edges and a central groove, while on the molars, the parastyle is narrow with no central groove. The metastyle becomes wide only on the premolars. The labial walls of the paracone and metacone are concave, with right-angled anterior and posterior corners. The anterio-exterior horn of the postfossette is longer than the posterio-exterior horn of the prefossette, even on the molars. The paraconid of p2 is lingually expanded and divided from the protoconid by marked lingual and labial constrictions; the metaconid is small and rounded, and the metastylid is large; the lingual valley is narrowly U-shaped; the labial wall of the hypoconid is flat, and the lingual wall has some plications; the entoconid is large and podiform; the postflexid is long and curved; the labial valley is deep and penetrates into the isthmus; and the pli caballinid is fine. The metastylid on p3 and p4 has some plications on its posterior wall, and its lingual end is at the same level with the metaconid; the lingual wall of the protoconid is roundly curved, developing anterior and posterior angles; the metaconid is narrowly rounded, with a wide and short neck; the metastylid is small and rounded, with a narrow and long neck; the lingual valley is narrowly U-shaped; the lingual wall of the hypoconid is wrinkled, while the labial wall is straight; the pli caballinid is narrow and long, and is located near the bottom of the labial valley; the labial valley is shallow, not penetrating into the isthmus; the entoconid is large and coracoid on p3, while it is small and podiform on p4. The double-knots on m1 and m2 are larger than those on p3 and p4, the pli caballinid is weaker, the labial valley is deep and penetrates into the isthmus, and the entoconid is small, rounded or roundly rectangular (Fig. 4h).

Hipparion hippidiodus is a medium-sized three-toed horse, with a length of 129 mm for its lower tooth row. On the lower cheek teeth, the labial wall is convex, lacking a protostylid; the labial valley is deep, penetrating into the isthmus; and the double-knots are rounded. The paraconid and protoconid of p2 are lingually divided; the metaconid has a coracoid anterior end; the metastylid has a short and narrow neck, and is more lingually shifted than the metaconid; the entoconid is coracoid; and the postflexid is long and curved. On p2 and p3, the anterior angle of the proflexid is distinct, but the posterior angle is weak; the metaconid has a long neck, and the metastylid has a narrow neck; and the pli caballinid is well-developed. On p3 and p4, the double-knots are relatively large and long, and are more lingually prominent than is the entoconid, but are weaker than those of the Qingyang specimens (Qiu et al., 1987, fig. 52); the lingual valley is widely and deeply V-shaped; the pro- and post-flexids are narrow and long; the protoconid and hypoconid are relatively wide, closing to the width of the double-knots; the entoconid is large and nearly square. On m1 and m2, the double-knots are small and the pli caballinid is absent. The lingual wall of the protoconid of m1 is strongly concave, and the entoconid and hypoconulid are narrow and long, with a constricted base.

Hipparion platyodus: on the upper cheek teeth of this three-toed horse, the protocone is large and narrow, with a convex lingual wall and sharp anterior and posterior ends; the plications are medially-developed; the labial and lingual walls of the paracone and metacone are flat; the parastyle is wide, with a marked posterior edge; the mesostyle is narrow, with a higher anterior wall than the posterior wall; the hypoconal groove is deep and sharp, and lacks a hypoconal constriction; and the pli caballine is small and frequently biforked. The anterostyle of P2 is wide and short, with a rounded end; the protocone is roundly rectangular, with a flat lingual margin; the parastyle is wide, and the mesostyle is centrally-grooved. P3 and P4 are very similar to each other: the parastyle is moderately wide, is slightly wider than the high and narrow mesostyle, and the protocone is large and rounded. M1–2 have some differences from P3–4: the lingual and labial walls of the para- and meta-cones are convex, the protocone is flatter and longer, and the parastyle is narrower than the mesostyle. The parastyle of M3 is weak, and the protocone is flat and long, and is semicircular in shape (Fig. 4g).

Hipparion licenti: the skull of this three-toed horse has a deep preorbital fossa that is strongly retracted so that its position is high and backward, and is located above the front of the orbit; its posterior border is located slightly anterior to the anterior rim of the orbit and posterior to the level of M3, and its lower border is at the same level with the upper rim of the orbit. A vertical ridge divides the preorbital fossa into two parts: the posterior part has a clear boundary, with no trace of the fossa foramen, but the anterior part has no clear boundary so that the maxillary bone forms a depression in this position. The orbit is slightly longer than high. The lacrymal notch is obvious, but does not form a foramen.

Shansirhinus ringstroemi: the skull of this acerathere rhino from Duikang has well-developed flanged parietal crests that are slowly posteriorly convergent, and their posterior parts are divergent toward the lateral ends of the occipital crest, connecting its lateral margins. The parietal crests are nearly parallel to each other on the parietal area, with a minimal width of 52.8 mm between them. The mandibular symphysis has a moderate width, with a deeply concave labial surface and a shallowly concave lingual surface. The i2 are small tusks, even smaller than the i2 of the female *Chilotherium*, with a distance of 91.5 mm between them. The wearing facet of i2 is located on the posterio-labial side, and the medial flanges turn upward. The nasals are long, with rough tips and a shallow and wide sagittal groove. The zygomatic arches are wide. The braincase is narrow with steep outer walls. On the upper premolars, the bridge is well-developed, the crista and crochet are slender, forming a medifossette, the parastyle is protruding, the paracone rib is absent, the connection between the protoloph and ectoloph is narrow, the protocone is strongly constricted, and the antecrochet is robust.

Hesperotherium sp.: the juvenile skull and mandible of this chalicothere from Duikang have DP2-4, dp2-4 and erupting M1. The nasals are wide at the back and contact with the lacrymals. The mandibular horizontal rami are shallow, and the posterior boundary of the symphysis is located before dp2. All teeth are brachyodont. DP1 and dp1 are absent. DP2 is triangular. DP3 and DP4 are quadrate. The protoconule and protoloph are developed on the upper milk-teeth. The lower milk-teeth consist of double "V". The labial cingula of the all cheek teeth are well-developed.

Ancylotherium sp.: the skull of this chalicothere from Duikang belongs to a juvenile individual with a cranial length of over 450 mm (Fig. 4e). The nasals are narrow, with a well-developed sagittal groove and vertical lateral surfaces. The central part of the frontal area is convex, and the maxillary face is long and flat. The preorbital fossa is rectangular and very shallow, and is located above DP4. The facial region of the lacrymal bone is approximately triangular and shallowly concave. The lower rim of the orbit is flat and the upper rim is curved. The postorbital process of the frontal bone is prominent and sharp at its tip. The supraorbital foramen is large and round. The temporal fossa is long and the zygomatic arch is thick. The occipital surface is triangular in shape, with a high central ridge. The postglenoid process is transversely flat and triangular in shape. The tympanic bulla is longitudinally extended, and is located at the interior side of the postglenoid process. The temporal condyle is flat and wide, and the pterygoid process is thin and high. The cheek teeth are high-crowned, with strong cingula. DP1 is absent. P2 is triangular in shape, with a convex labial wall; the ectoloph is narrow, and the protoloph is slender and posteriorly oblique; the anterior cingulum becomes a broad platform; and the protocone is expanded. DP3 is nearly square, with a continuous lingual cingulum and a rounded protocone. DP4 is rectangular in shape, with a strongly wavy labial wall; the mesostyle is strongly prominent and forms a plate, but is reduced toward the root; the parastyle is markedly prominent; the para- and meta-cones do not exceed the midline; the protocone is expanded and rounded, and the hypocone is small; the protoloph is nearly transverse, and the metaloph is slightly posteriorly oblique; the crochet is slender and the cingula are well-developed. M1 is rectangular, with a marked W-shaped ectoloph; the para- and meso-styles are prominent and form plates; the para- and meta-cones exceed the midline; the protocone is a large cone, and the hypocone is weak; the protoloph and metaloph are nearly parallel to each other and are slightly posteriorly oblique; the crochet is marked; the labial cingulum is weak, but the lingual cingulum is high and thick and extends to the labial half of the anterior and posterior sides of the tooth.

Palaeotragus microdon is a medium-sized giraffid, represented by a skull and a maxillary from Duikang. The maxillary face is short and the orbit is vertically-positioned and oval in shape. Horns are located above the orbit, and are slender and straight, sharpening upward. The basal parts of the horns have grooves, becoming smooth in an upward direction. The lateral surfaces of the nasals are slightly convex. The upper cheek teeth are square in outline, with well-developed parastyles and mesostyles. The exterior ridge of the paracone has a marked and rounded edge, and that of the metacone is centrally-grooved. The anterior tips of the protocone and metaconule are not curved. The lingual crescent lophs are simple and lack an entostyle and lingual cingulum. The p4 has a rounded medial vertical edge, and anterior and posterior folds.

Cervavitus novorossiae: the antler of this deer has marked grooves and ridges on its surface. The main beam and brow tine are slightly curved. The burr is notably bulged, consisting of a series of tuberculiform nodules of different sizes. The brow tine is highly positioned above the burr, with a distance of 126 mm between them. The connection between the main beam and brow tine is weakly palmate. The brow tine has a length of 130 mm and is at a 50° angle to the main beam. The base of the main beam is oval in cross-section with a short diameter of 25 mm.

Sinotragus sp.: the skull of this bovid from Duikang has an angle of over 60° between facial and cranial axes. The frontal area is centrally flat and laterally curved, and lacks a supraorbital foramen. The cranial region is short and wide, with a slightly convex roof. The lacrymal fossa is large and

deep, and extends to the infraorbital foramen that is located 2.5 cm above P3. The facial region of the lacrymal bone is nearly equal to that of the zygomatic bone. The orbital rims are moderately prominent and the dentition is located in front of the orbit. The occipital surface is broad, with a distinct central crest. In ventral view, the occipital base is short and quadrangular, the sagittal groove is deep, and both of the anterior and posterior basal tuberosities are transversely prominent. The horn cores are located above the posterior region of the orbit, are moderately long, posteriorly oblique, and strongly inferiorly curved; the cross section of the base is approximately triangular, rapidly becoming superiorly narrow; the rotation is clear, about 90° in a clockwise direction (right horn); the bases of the horn cores are very close to each other, and the lower two-thirds are nearly parallel to each other on their medial sides, while the upper thirds are distinctly divergent; the lateral surface is very rough, with marked grooves on the anterio-lateral side, among which a deep groove extends from the horn base to the tip; the medial surface is very flat, with many fine grooves that extend upward; the anterior edge begins sharpening from 9 cm above the horn base; the posterior edge is rounded. The cheek teeth are wide and low-crowned. The premolars are long. P3 is longer than P2, and P4 is very short, with a well-developed parastyle. The molars have well-developed parastyles, weak ribs, and frequent enamel islands between the anterior and posterior lobes.

Gazella blacki is a large-size gazelle with high-crowned teeth. The horn corns are robust and curved, and the horn bases are close to each other and moderately divergent and rapidly sharpened from base to tip. On the horn surface, ridges are clear, and grooves are deep and dense. The outline of the horn core base is oval in shape, with a width of 24 mm, and the longitudinal axis is slightly longer than the transverse axis. The p4 has a high metaconid, connecting the expansion of the paraconid, and both are parallel to each other, forming a U-shape. The crown height index of m1 (length/height × 100) is 109.

Several proboscideans of the Gaozhuang Fauna, such as *Mammut borsoni, Anancus sinensis,* and *Sinomastodon intermedius*, which lived in warm and humid conditions, have not been found in the Duikang locality or the Shilidun Fauna. Micromammals of the Shilidun Fauna have not been systematically collected and only skulls of porcupines and lagomorphs have been found until now. Two giraffids, *Palaeotragus microdon* and *Samotherium* sp., as well as chalicotheres, were found from Duikang. Chalicotheres have not been found in the Gaozhuang Fauna. All of these herbivores are typical browsers. The components of the Shilidun Fauna indicate that the environment of the Linxia Basin was a subarid steppe during the Early Pliocene.

5 Mio-Pliocene Boundary at the Duikang Section

Li et al. (1984) correlated the Jinglean Age, which was considered to belong to the Early Pliocene, to the Ruscinian Age of the European land mammal ages, corresponding to MN 14–15. Its mammalian localities or assemblages include Hefeng in Jingle, Shanxi, Zone II in Yushe, Shanxi, and Leijiahe in Lingtai, Gansu. The Gaozhuang Age was created by Qiu et al. (1987), but was later replaced by the Yushean Age (Qiu and Qiu, 1990). They suggested that the Early Pliocene part of the Yushean Age was represented by the Gaozhuang Fauna, corresponding to the European Ruscinian Age, and its contemporaneous mammals included the Harr Obo Fauna in Huade, Inner Mongolia, which was correlated to the fossil assemblage of the basal part of the Gaozhuang Formation, and the Bilike Fauna in Huade, which was correlated to the late Gaozhuang Fauna. Tong et al. (1995) reconfirmed the correlation of the Yushean Age to the European Ruscinian and early Villanyian ages, representing the whole Pliocene.

In 1999, the Second All-China Stratigraphic Commission (ACSC) formally proposed to establish the chronostratigraphic units of the Chinese Pliocene, the Gaozhuangian and Mazegouan stages, in which the time spans correspond to the Gaozhuangian and Mazegouan ages of the Chinese land mammal ages (ACSC, 2001). Since then, the Gaozhuangian Age (Stage) has been reintroduced. At the same time, the Mazegouan Age (Stage) was newly nominated. Deng (2006) correlated the Gaozhuangian and Mazegouan ages to the Ruscinian and early Villanyian ages, respectively.

According to the definition proposed by ACSC (2001), the Chinese terrestrial Gaozhuangian Stage of the Lower Pliocene should be correlated to the marine Zanclean Stage of the International Stratigraphical Chart, and the Gaozhuangian Age should be correlated to the Ruscinian Age of the Europe land mammal ages. The lower boundary of the Zanclean is situated at the upper part of Chron C3r, and is 96 ka earlier than the Thvera normal subchron (C3n.4n), with an astronomical age of 5.332 Ma in the orbitally-calibrated time scale. Its calcareous nannofossils (coccoliths) are close to the disappearance of *Triquetrorhabdulus rugosus* (base of CN10b) and the first occurrence of *Ceratolithus acutus*. GSSP of the Zanclean Stage is located in the Eraclea Minoa section on the southern coast of Sicily, Italy, at the base of the Trubi Formation (base of the carbonate bed marking the small-scale stratigraphic cycle (1), ratified by IUGS in 2000 (Van Couvering et al., 2000). The lower boundary of the Ruscinian is also at the upper part of Chron C3r, with an age of 5.3 Ma (Steininger et al., 1996). As a result, the

lower boundary of the Gaozhuangian Stage is identical with those of the Zanclean and Ruscinian, and is located at the upper part of Chron C3r, with an age of 5.3 Ma (Deng, 2006).

According to the chronostratigraphical subdivision of the Chinese Neogene (Deng, 2002, 2006), the Duikang section includes the Miocene/Pliocene boundary, i.e., the lower boundary of the Gaozhuangian Stage. The first occurrence of *Hipparion* (*Proboscidipparion*) *pater* (0.8 m above the lower boundary of the Hewangjia Formation) is a biostratigraphical marker, below which it belongs to the Late Miocene Baodean Stage, and above which it belongs to the Early Pliocene Gaozhuangian Stage.

Among the first appeared large mammals at Duikang, *Hipparion pater* is smaller in size than *H. sinense* of the Early Pleistocene. The nasals of the former are less reduced than those of the latter, the tooth crowns are lower, the plications of the fossettes are fewer, the para- and meso-styles are narrower, and the lateral walls of the lower premolars are more convex. Besides the Duikang material, *H. pater* was also found at Gaozhuang in Yushe, Shanxi, Loc. 5 in the northern region of Baode, Shanxi, and Youhe in Weinan, Shaanxi (Qiu et al., 1987). *Chasmaporthetes* first appeared during the middle Late Miocene in Europe, but appeared in Asia from the Pliocene. Besides the distribution at Duikang and Shilidun in Guanghe, Gansu, *Chasmaporthetes kani* was found at the Pliocene localities of Gaozhuang and Catacombs in Odessa, Ukraine (Qiu et al., 2004a).

Among the last appeared taxa, *Alilepus annectens* first appeared at Ertemte in Huade, Inner Mongolia, and continued into Gaozhuang in Yushe, Shanxi, and Harr Obo in Huade, Inner Mongolia (Storch, 1987; Qiu, 1987; Flynn et al., 1997). *Hipparion platyodus* appeared from the Late Miocene Baodean Age, and was distributed in Wuxiang, Shanxi, and Wudu, Gansu. *H. platyodus* is very common from the Mahui Formation to the Gaozhuang Formation in the Yushe Basin, and it may be the ancestor type of *H. houfenense* (Qiu et al., 1987).

The above-mentioned comparisons seem to show that the age of the Duikang mammals or Shilidun Fauna is slightly earlier than that of the Gaozhuang Fauna. The markers of the lower boundary of the Pliocene or Gaozhuangian Stage in the Duikang section are relatively rich. However, it is very difficult to determine the first or last appearance of a species independently. Coexistence of first and last appeared species is a good method to resolve this issue (Deng et al., 2007). Among the above-mentioned fossils, either of the first appeared species *Hipparion pater* and *Chasmaporthetes kani* combines with either of the last appeared species *Alilepus annectens* and *Hipparion platyodus*, providing an important reference to judge the lower boundary of the Pliocene or Gaozhuangian Stage.

6 Magnetostratigraphy

Li et al. (1995) and Fang et al. (1997, 2003) provided paleomagnetic dates for the Linxia sequence, including the Maogou, Wangjiashan, and Dongshanding sections. Samples were taken at 0.5–1.0 or 2.0 m stratigraphic intervals, along 1 m deep trenches through the entire length of the sections. Exceptions were made for the conglomerates, where sampling intervals depended on the availability of finer-grained lenses. These sections include paleomagnetic measurements of the Liushu and Hewangjia formations.

Paleomagnetic results for the Maogou and Wangjiashan sections show that the Hewangjia Formation records four normal and three reversed magnetozones (Fang et al., 2003, fig.3). From bottom to top, the long first normal zone, which extends into the Liushu Formation, was correlated to C3An, and the long first reversed zone to C3r. The short second and third normal zones, and the long fourth normal zone, which extends into the Jishi Formation, were correlated to C3n.4n, C3n.1n, and C2An.3n, respectively. As a result, the upper part of C3r as marks of the lower boundary of the Gaozhuangian Stage, and a precise position dated 0.1 Ma earlier than C3n.4n is situated within the basal red clays of the Hewangjia Formation, with an age of 5.3 Ma. According to the paleomagnetic measurements, the Early Pliocene Shilidun Fauna, which includes the fossils from Duikang, is within C3n.4n, with an age of 5.0 Ma, corresponding to MN 14 of Europe.

7 Stable Isotopes

According to the age data, the lower boundary of the Gaozhuangian Stage should be well correlated to the global expansion of C_4 plants, which have been shown in Siwaliks, North America, and East Africa as well as Yushe, Shanxi and central Inner Mongolia in China (Hou et al., 2006; Zhang et al., 2009). On the other hand, the carbon isotopic record from analyses of fossil tooth enamel and soils from the Linxia Basin indicates that the $\delta^{13}C$ values of tooth enamel prior to the Pleistocene display a narrow range of variation from −8.4‰ to −12.4‰, with a mean $\delta^{13}C$ value of −10.0‰ (Wang and Deng, 2005). These $\delta^{13}C$ values indicate that these various herbivores were feeding predominantly on C_3 plants during the late Paleogene and Neogene. The pure or nearly pure C_3 diet of various herbivores suggests that the ecosystems in the Linxia Basin consisted primarily of C_3 plants prior to ~2–3 Ma. The $\delta^{13}C$ values of herbivore tooth enamel from the Linxia Basin for this time interval correspond to a dietary intake of −22.4‰

to −26.4‰, with a mean value of −24.0‰, which falls well within the $\delta^{13}C$ range of modern C_3 plants. The enriched $\delta^{13}C$ values for herbivores' diets in the Linxia Basin (based on the analysis of fossil enamel) relative to the mean $\delta^{13}C$ value for C_3 plants suggest that water-stressed conditions are not a recent phenomenon in the area and probably have existed in the Linxia Basin since the Late Oligocene. The carbon isotope data from the Linxia Basin do not show a positive $\delta^{13}C$ shift in the Late Miocene or Early Pliocene. The mean enamel $\delta^{13}C$ value prior to 7 Ma is −9.9‰ and is indistinguishable from the mean $\delta^{13}C$ of −10‰ for the period of 7.0 to 2.5 Ma.

The $\delta^{18}O$ of tooth enamel is related to the $\delta^{18}O$ of local meteoric water, which provides drinking water for most animals and water for plants that are consumed by herbivores. Because the $\delta^{18}O$ of meteoric water is controlled by climatic conditions, a shift in $\delta^{18}O$ of tooth enamel of the same species indicates a change in some aspects of regional climate. The large range of $\delta^{18}O$ values within the horse and rhino families at a given time interval may reflect differences in the drinking and dietary behaviors of different species and seasonal variability of $\delta^{18}O$ of local rainfall. Near the Miocene/Pliocene boundary of the Linxia Basin, the $\delta^{18}O$ of tooth enamel from horses shifted significantly to more negative values after ~6 Ma. This negative oxygen isotopic shift indicates changes in climate towards cooler temperatures and/or less arid conditions. Similarly, there is a significant $\delta^{18}O$ shift towards higher values after ~7, which indicates a shift to warmer and/or drier conditions. The enamel $\delta^{18}O$ values from rhinos of the Linxia Basin also show parallel shifts where there is data coverage. Most notably, the positive $\delta^{18}O$ shift after ~7 Ma, which is also seen in deer and bovid of the Linxia Basin, is comparable in timing and direction to the $\delta^{18}O$ shift observed in paleosol carbonates and fossil enamel in Pakistan and Nepal (Quade et al., 1989; 1992; 1995), indicating a change in climatic conditions on both sides of the plateau at about the same time in the Late Miocene. The tooth-enamel $\delta^{18}O$ data from the Linxia Basin show a general shift to more negative values from about ~6 to ~2.5 Ma, indicating a shift to cooler temperatures. This is in broad agreement with the marine $\delta^{18}O$ and Mg/Ca records (Lear et al., 2000; Zachos et al., 2001).

Acknowledgements

We thank Professors Qiu Zhanxiang, Wang Banyue, Fang Xiaomin, and Song Chunhui for their supports in fieldwork, and Dr. Dana Biasatti for her improvement in English. This work was supported by the Ministry of Science and Technology of China (2006FY120300 and 2006CB806400), the Knowledge Innovation Program of the Chinese Academy of Sciences (KZCX2-YW-120, Q09), the National Natural Science Foundation of China (40730210), and the All-China Stratigraphic Commission.

Manuscript received May 4, 2010
accepted Sept. 15, 2010
edited by Jiang Shaoqing

References

All-China Stratigraphic Commission, 2001. *Chinese Stratigraphic Guide and Its Introduction*. Beijing: Geological Publishing House, 1–59 (in Chinese).

Chen Xiaofeng, 1994. Stratigraphy and large mammals of the "Jinglean" Stage, Shanxi, China. *Quaternary Sciences*, (4): 339–353 (in Chinese with English abstract).

Deng Tao, 2002. Neogene. In: All-China Stratigraphic Commission (Ed), *Instruction for the Chinese Regional Chronostratigraphic Scale (Geological Time)*. Beijing: Geological Publishing House, 12–15 (in Chinese).

Deng, T., 2005. New cranial material of *Shansirhinus* (Rhinocerotidae, Perissodactyla) from the Lower Pliocene of the Linxia Basin in Gansu, China. *Geobios*, 38: 301–313.

Deng Tao, 2006. Chinese Neogene mammal biochronology. *Vertebrata PalAsiatica*, 44(2): 143–163.

Deng Tao, 2009. Late Cenozoic environmental change in the Linxia Basin (Gansu, China) as indicated by mammalian cenograms. *Vertebrata PalAsiatica*, 47(4): 282–298.

Deng Tao, Hou Sukuan and Wang Hongjiang, 2007. The Tunggurian Stage of the continental Miocene in China. *Acta Geologica Sinica* (English edition), 81(5): 709–721.

Deng Tao, Hou Sukuan, Wang Taiming and Mu Yongqing, 2010. The Gaozhuangian Stage of the continental Pliocene Series in China. *Journal of Stratigraphy*, 34(3): 225–240 (in Chinese with English abstract).

Deng Tao, Wang Xiaoming, Ni Xijun and Liu Liping, 2004a. Sequence of the Cenozoic mammalian faunas of the Linxia Basin in Gansu, China. *Acta Geologica Sinica* (English edition), 78(1): 8–14.

Deng Tao, Wang Xiaoming, Ni Xijun, Liu Liping and Liang Zhong, 2004b. Cenozoic stratigraphic sequence of the Linxia Basin in Gansu, China and its evidence from mammal fossils. *Vertebrata PalAsiatica*, 42(1): 45–66 (in Chinese with English summary).

Ding, Z.L., Sun, J.M., Liu, T.S., Zhu, R.X., Yang, S.L., and Guo, B., 1998. Wind-blown origin of the Pliocene red clay formation in the central Loess Plateau, China. *Earth and Planetary Science Letters*, 161: 135–143.

Fang, X.M., Garzione, C., van der Voo, R., Li, J.J., and Fan, M.J., 2003. Flexural subsidence by 29 Ma on the NE edge of Tibet from the magnetostratigraphy of Linxia Basin, China. *Earth and Planetary Science Letters*, 210: 545–560.

Fang Xiaomin, Li Jijun, Zhu Junjie, Chen Huailu and Cao Jixiu, 1997. Division and age dating of the Cenozoic strata of the Linxia Basin in Gansu, China. *Chinese Science Bulletin*, 42 (14): 1457–1471 (in Chinese).

Flynn, L.J., Tedford, R.H., and Qiu, Z.X., 1991. Enrichment and stability in the Pliocene mammalian fauna of North China. *Paleobiology*, 17: 246–265.

Flynn, L.J., Wu, W.Y., and Downs, W.R., 1997. Dating vertebrate

microfaunas in the late Neogene record of northern China. *Palaeogeography, Palaeoclimatology, Palaeoecology*, 133: 227–242.

Guo, Z.T., Peng, S.Z., Hao, Q.Z., Biscaye, P.E., and Liu, T.S., 2001. Origin of the Miocene-Pliocene red-earth formation at Xifeng in northern China and implications for paleoenvironments. *Palaeogeography, Palaeoclimatology, Palaeoecology*, 170: 11–26.

Hou Sukuan, Deng Tao and Wang Yang, 2006. Stable carbon isotopic evidence of tooth enamel for the late Neogene habitats of the *Hipparion* fauna in China. In: Dong, W. (Ed), *Proceedings of the Tenth Annual Meeting of the Chinese Society of Vertebrate Paleontology*. Beijing: China Ocean Press, 85–94 (in Chinese with English abstract).

Lear, C., Elderfield, H., and Wilson, P., 2000. Cenozoic deep-sea temperatures and global ice volumes from Mg/Ca in benthic foraminiferal calcite. *Science*, 287: 269–272.

Li Chuankui, Wu Wenyu and Qiu Zhuding, 1984. Chinese Neogene: subdivision and correlation. *Vertebrata PalAsiatica*, 22(3): 163–178 (in Chinese with English summary).

Li, J.J., et al., 1995. *Uplift of Qinghai-Xizang (Tibet) Plateau and Global Change*. Lanzhou: Lanzhou University Press, 1–207.

Licent, E., and Trassaert, M., 1935. The Pliocene lacustrine series in central Shansi. *Bulletin of the Geological Society of China*, 14: 211–219.

Protophyllocladoxylon jingyuanense sp. nov., a Gymnospermous Wood of the Serpukhovian (Late Mississippian) from Gansu, Northwest China. *Acta Geologica Sinica* (English edition), 84 (2): 257–268.

Qiu, Z.D., 1987. The Neogene mammalian faunas of Ertemte and Harr Obo in Inner Mongolia (Nei Mongol), China. 6. Hares and pikas (Logomorpha: Leporidae and Ochotonidae). *Senckenbergiana Lethaea*, 67: 325–399.

Qiu, Z.X., 1987. Die Hyaeniden aus dem Ruscinium und Villafranchium Chinas. *Munchner Geowissenschaftliche Abhandlungen*, 9: 1–109.

Qiu Zhanxiang, Deng Tao and Wang Banyue, 2004a. Early Pleistocene mammalian fauna from Longdan, Dongxiang, Gansu, China. *Palaeontologia Sinica*, New Series C, 27: 1–198 (in Chinese with English summary).

Qiu Zhanxiang, Huang Weilong and Guo Zhihui, 1987. The Chinese hipparionine fossils. *Palaeontologia Sinica*, New Series C, 25: 1–250 (in Chinese with English summary).

Qiu Zhanxiang and Qiu Zhuding, 1990. Neogene local mammalian faunas: succession and ages. *Journal of Stratigraphy*, 14(4): 241–260 (in Chinese).

Qiu Zhanxiang, Wang Banyue and Deng Tao, 2004b. Mammal fossils from Yagou, Linxia Basin, Gansu, and related stratigraphic problems. *Vertebrata PalAsiatica*, 42(4): 276–296 (in Chinese with English summary).

Qiu Zhanxiang, Xie Junyi and Yan Defa, 1990. Discovery of some Early Miocene mammalian fossils from Dongxiang, Gansu. *Vertebrata PalAsiatica*, 28: 9–24 (in Chinese with English summary).

Quade, J., Carter, J., Ojha, T., Adams, J., Harrison, T., 1995. Late Miocene environmental change in Nepal and the northern Indian subcontinent: stable isotopic evidence from paleosols. *Geological Society of America Bulletin*, 107: 1381–1397.

Quade, J., Cerling, T.E., Barry, J., Morgan, M., Pilbeam, D., Chivas, A., Lee-Thorp, J., and van der Merwe, N., 1992. A 16-Ma record of paleodiet using carbon and oxygen isotopes in fossil teeth from Pakistan. *Chemical Geology*, 94: 183–192.

Quade, J., Cerling, T.E., and Bowman, J.R., 1989. Development of Asian monsoon revealed by marked ecological shift during latest Miocene in northern Pakistan. *Nature*, 342: 163–166.

Steininger, F.F., Berggren, W.A., Kent, D.V., Bernor, R.L., Sen, S., and Agusti, J., 1996. Circum-Mediterranean Neogene (Miocene and Pliocene) marine-continental chronologic correlations of European mammal units. In: Bernor, R.L., Fahlbusch, V., and Mittmann, H.W. (Eds), *The Evolution of Western Eurasian Neogene Mammal Faunas*. New York: Columbia University Press, 7–46.

Storch, G., 1987. The Neogene mammalian faunas of Ertemte and Harr Obo in Inner Mongolia (Nei Mongol), China. 7. Muridae (Rodentia). *Senckenbergiana Lethaea*, 67: 407–409.

Teilhard de Chardin, P., and Young, C.C., 1930. Preliminary observations on the pre-Loessic and post-Pontian formations in western Shansi and northern Shensi. *Memoir of the Geological Survey of China*, Series A, 8: 1–54.

Teilhard de Chardin, P., and Young, C.C., 1933. The Late Cenozoic formation of S. E. Shansi. *Bulletin of the Geological Society of China*, 12: 207–248.

Tong Yongsheng, Zheng Shaohua and Qiu Zhuding, 1995. Cenozoic mammal ages of China. *Vertebrata PalAsiatica*, 33 (4): 290–314 (in Chinese with English summary).

Van Couvering, J.A., Castradori, D., Cita, M.B., Hilgen, F.J., and Rio, D., 2000. The base of the Zanclean Stage and of the Plioeene Series. *Episodes*, 23: 179–187.

Wang, Y., and Deng, T., 2005. A 25-Ma record of paleodiet and environmental change from carbon and oxygen isotopes in mammalian tooth enamel and paleosols from the NE margin of the Tibetan Plateau. *Earth and Planetary Science Letters*, 236: 322–338.

Yue Leping and Zhang Yunxiang, 1998. *Hipparion* fauna and magnetostratigraphy in Hefeng, Jingle, Shanxi Province. *Vertebrata PalAsiatica*, 36(1): 76–80 (in Chinese with English summary).

Zachos, J., Pagani, M., Sloan, L., Thomas, E., and Billups, K., 2001. Trends, rhythms, and aberrations in global climate 65 Ma to present. *Science*, 292: 686–693.

Zdansky, O., 1924. Jungtertiäre Carnivoren Chinas. *Palaeontologuia Sinica*, Series C, 2(1): 1–150.

Zhang, C.F., Wang, Y., Deng, T., Wang, X.M., Biasatti, D., Xu, Y.F., and Li, Q., 2009. C4 expansion in the central Inner Mongolia during the latest Miocene and Early Pliocene. *Earth and Planetary Science Letters*, 287: 311–319.

Zhang Yunxiang, Sun Donghuai, An Zhisheng and Xue Xiangxu, 1999. Mammalian fossils from Late Pliocene (lower MN 16) of Lingtai, Gansu Province. *Vertebrata PalAsiatica*, 37(3): 190–199 (in Chinese with English summary).